Gas Fueled RDE Scramjet

Gabriel Diez Cameron Ellis Alberto Marin Cebrian Andrew McClaskey
Thomas Satterly Drew Sherman

December 15, 2017

Contents

1 Abstract

Hypersonic vehicles demand high performance from every subsystem, with emphasis on a stable propulsion system and material capabilities. This project aims to investigate the feasibility of using a gas-fueled Rotating Detonation Engine (RDE) in a hypersonic vehicle with a cruise Mach of 6.5 at 1500 psf of dynamic pressure, launched on the GO1 platform. It was found that an ethylene fueled RDE, paired with a conical inlet and various cooling systems, is potentially capable of 107 seconds of flight, 45 second of which at cruise velocity. Most notable is a cruise Isp of 2080 seconds, which is substantially higher than conventional scramjet burners. The preliminary design shows that, while an RDE may be feasible for such a mission, extensive fundamental research is required to fully understand the operation of an RDE.

2 Introduction

Sustained air-breathing hypersonic flight has been the focus of a great deal of research over the past several decades. In addition to the high temperatures associated with flight speeds higher than Mach 5, it is difficult to slow down flow speed to subsonic speeds (such as in a ramjet) for sustainable combustion without significant pressure losses, making it necessary to design combustors that can burn at supersonic velocities. One proposal for improving supersonic combustion is to modify the mechanism of reaction all together. Deflagrations require sufficient mixing of fuel and oxidizer to initiate a reaction as well as transfer energy from that reaction to the incoming flow. This is simple to accomplish at low flow speeds but deflagration proves to be an unreliable reaction mechanism at supersonic velocities. Detonations, on the other hand, are supersonic waves that flow through combustible material, reacting it as it passes [1]. Rotating Detonation Engines (RDE) have shown great promise over recent years due to their ability to maintain combustion at higher Mach numbers than traditional scramjet engines. By maintaining one or multiple detonation waves within the burner, the combustor is able to produce much higher average chamber pressures. [2] Additionally, since detonation reactions occur almost instantaneously, the combustion chamber itself can be shortened compared to traditional supersonic burners. The objective of the current work is to propose a design for a gas-injection RDE scramjet intended to be launched from a GO1 launcher to complete a cruising mission at hypersonic velocities. The GO1 is capable of reaching velocities as high as Mach 5 and the fairing requires the vehicle not exceed 24" in diameter and 120" in length.

3 Design Methodology

3.1 Mission Design and Constraints

3.2 Vehicle Trajectory [Andy McClaskey]

The design of this vehicle was based on a 1500 pounds per square foot (71.82 kPa) constant dynamic pressure trajectory. The trajectory was found by iterating Mach number to make the density given in the dynamic pressure equation match that given by the standard atmosphere function. The altitude and velocity trajectory are shown below in Figure 1 and Figure 2.

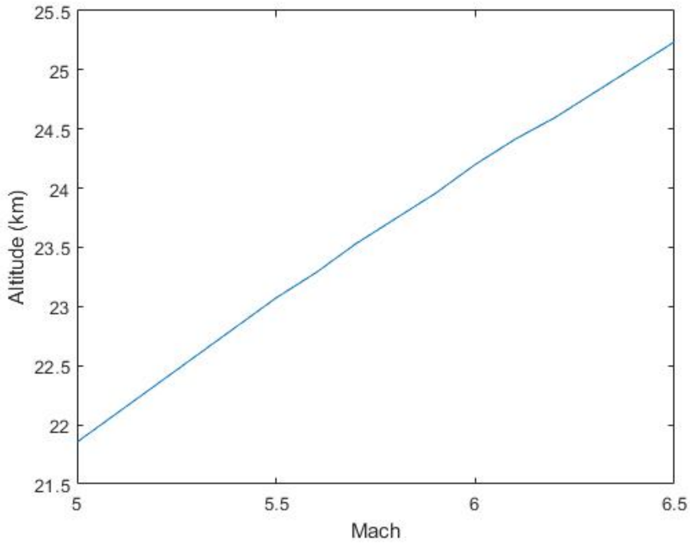

Figure 1: Altitude v. Mach

The end point shown in Figure 1 and Figure 2 are the cruise conditions for this mission.

3.3 Aerodynamic Performance Analysis [Andy McClaskey]

Aerodynamic Reference Area The reference area needed for calculated lift and drag was determined by assuming a trapezoidal wing planform. The root and tip chord length were used as inputs to the area equation to calculate the wing planform area. The equation used for calculation total wing area is shown in Equation 1.

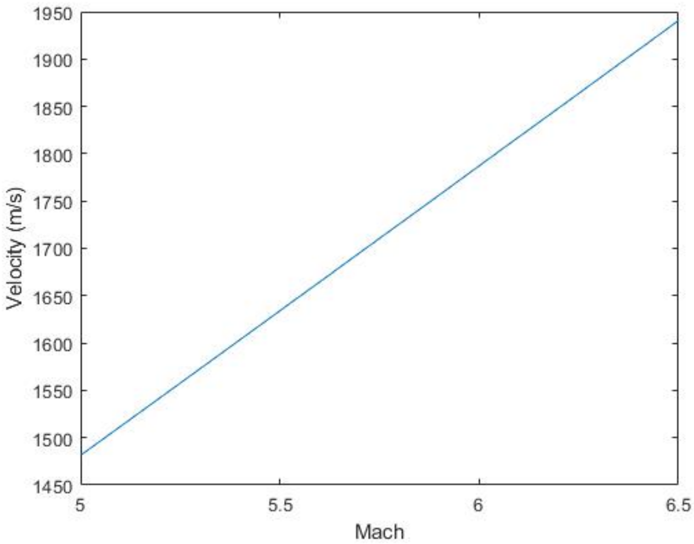

Figure 2: Velocity v. Mach

$$S = (\text{Root Chord}+\text{Tip Chord})*\frac{\text{Wing Span}}{2} \tag{1}$$

The planform was optimized for a drag to help increase the lift to drag ratio later in the design

Drag Determination The Coefficient of Drag (C_D) was taken from the 1x scale Generic Hypersonic Vehicle [9] for the angle of attack of zero. Once the coefficient of drag was known, the total drag could be calculated using Equation 2. They dynamic pressure is known from the free stream conditions of the vehicle and the aero reference area is known from above. The Coefficient of Drag is plotted in Figure 3.

$$D = q_\infty S C_D \tag{2}$$

Thrust Required The drag determined above sets the thrust required from the propulsion system for the vehicle in straight and level unaccelerated cruise flight. For the acceleration part of the mission the thrust required is shown in Equation 3. It was assumed that the pitch angle was close to zero for this analysis.

$$\text{Thrust} = m\frac{dv}{dt} + D + mg\sin\theta \tag{3}$$

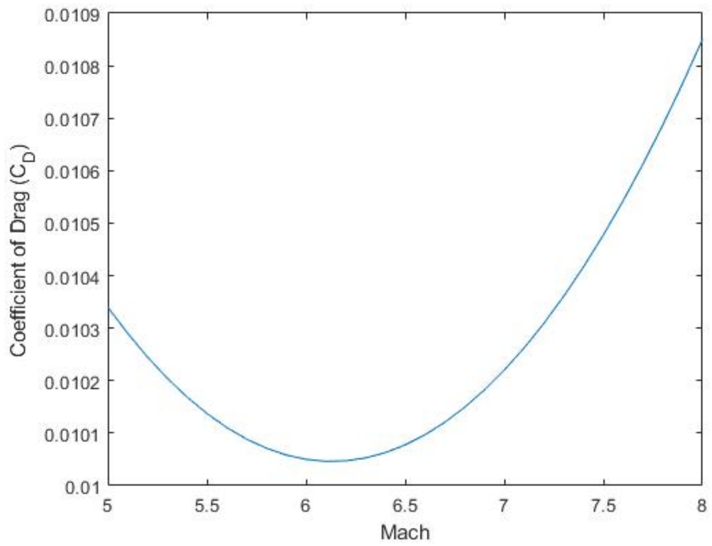

Figure 3: C_D v. Mach

Lift Determination In the cruise portion of the mission, the weight of the vehicle is known, we can determine the Coefficient of Lift required to support the vehicle. This is done using Equation 4.

$$C_L = \frac{\text{weight}}{q_\infty S} \tag{4}$$

Lift over Drag The Lift to Drag Ratio is calculated using Equation 5. Lift over drag is a primary input into the Bergeut range equation that can be used later for estimating the range. The Lift to Drag ratio is plotted in Figure 4. The drag was optimized to be at its minimum at our cruise condition. With more time, the component build up method could be used to determine if this drag estimate is accurate.

$$\text{Lift over Drag} = \frac{C_L}{C_D} \tag{5}$$

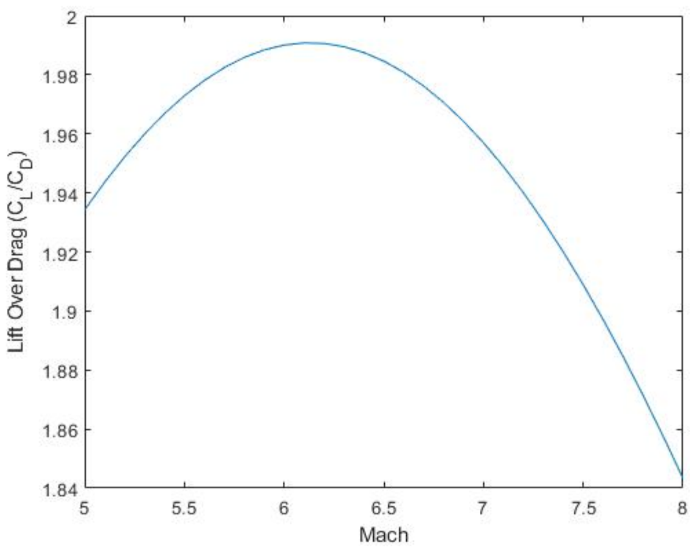

Figure 4: C_L/C_D v. Mach

3.4 Inlet, Isolator, and Compression Duct [Thomas Satterly]

Inlet The inlet was designed to provide the desired mass flow rate (3.5 kg/s) at cruise conditions whilst being capable of starting at Mach 5.5. Additionally, the geometry must be axisymmetric in order for a smooth flowpath from the inlet to the RDE. To satisfy these constraints, a simple conical inlet with variable geometry was selected. A cone with a half angle of 5 degrees was selected to minimize pressure loss and heat transfer at the inlet. By solving the Taylor-Maccoll equations for a conical shock, the outer cowl was sized to place the shock at the cowl during cruise conditions. In order to avoid mass flow loss and extra drag due to spillage at the starting conditions, a variable geometry cone is desirable to keep the shock at the cowl. This is achieved by shifting the inlet cone axially during acceleration. For this inlet to perform as desired between Mach 5.5 and 6.5, the cone only needs to be able to move 2.6 cm in total. The extremes of the cone position, as well as the shock placement on the cowl, can be seen in Figure 5.

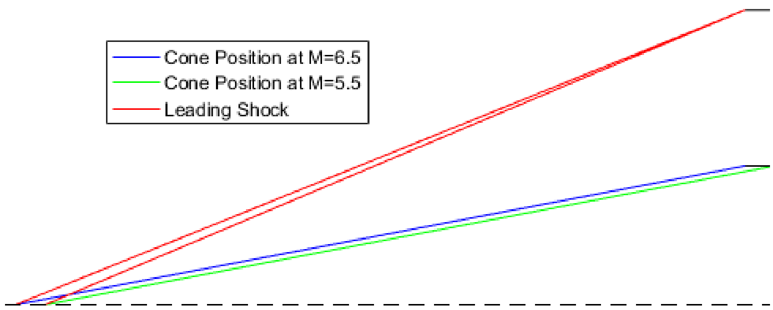

Figure 5: C_D v. Mach

Isolator The isolator was designed using a combination of industry accepted assumptions and correlations rather than a complete shock train analysis, given that this is a preliminary design. A constant area annular duct was chosen for the general geometry, as it would transition easily from the conical inlet and minimally disrupt the flow as it approaches the combustor. A major assumption made was that the exit Mach from the isolator is 1/2 of the entrance Mach to the inlet. Typically, this ratio is closer to 1/3, but a great advantage of the RDE is the possibility to maintain combustion at high Mach numbers. If this design exercise is to be forward-looking, it is not unreasonable to assume that more capable isolators will also be developed in the future. The total pressure ratio of the isolator is taken from MilStd 5007D [1], which is a relationship between free stream Mach and total pressure ratio that has been standardized to allow for preliminary design and sizing of an inlet and isolator system without spending valuable resources on an extensive flow analysis. Finally, the length of the inlet was derived using the Waltrup and Billig correlations [12]. The final isolator parameters are shown in table 3.4.

L/D	18
Mach Ratio	0.5
Total Pressure Ration	0.294

Compression Duct The final piece needed before reaching the combustor is a compression duct between the isolator and RDE entrance. The compression duct serves many purposes that ultimately balances the RDE operational properties with the upstream properties already set by the inlet and isolator system. The inlet sets the mass flow rate while the isolator sets the total pressure, total temperature, and Mach of the flow before reaching the compression duct. The RDE, on the other hand, was designed to operate at a specific static pressure, mass flow rate, and has a prescribed geometry. The compression duct unifies these components by delivering the flow from the inlet and isolator system, which have their own prescribed geometry, to the RDE such that flow properties are not violated. This was accomplished primarily by iterating on possible RDE operational conditions and geometry and verifying that, if the compression duct is isentropic, the upstream flow can be successfully delivered to the RDE within its design specifications.

3.5 Combustor [Thomas Satterly]

The chosen combustor was a gaseous ethylene fueled RDE. The sizing of the combustion chamber was based off of the Bykovskii [4] guidelines and experimentally observed cell sizes for gaseous ethylene [3]. Chapman-Jouget detonation parameters were calculated using the NASA CEA program, and the RDE performance was analyzed using the model proposed by Stechmann (REF XXX). The mass flow rate, minimum pressure, and minimum temperature were varied and the design iterated, along with the inlet, isolator, and compression duct, until a reasonable flow path was found with acceptable performance.

From experimental data collected by Bull et. al. [3], the approximate cell size of an ethylene-air mixture at 195 kPa is approximately 12.6 mm. From the guidelines given by Bykovskii in equations 6 through 9, the bounds on the RDE size can be calculated.

$$h \cong (12 \pm 5)a \tag{6}$$

$$(d_c)_{min} = \frac{h(7 \pm 2)}{\pi} \tag{7}$$

$$L_{min} \cong 2h \tag{8}$$

$$\Delta \cong 0.2h \tag{9}$$

From these guidelines, the RDE outer diameter was chosen at 0.2035 m with an inner diameter of 0.16 m and a total length of 0.254 m. A CAD model of the combustor can be seen in figure 6.

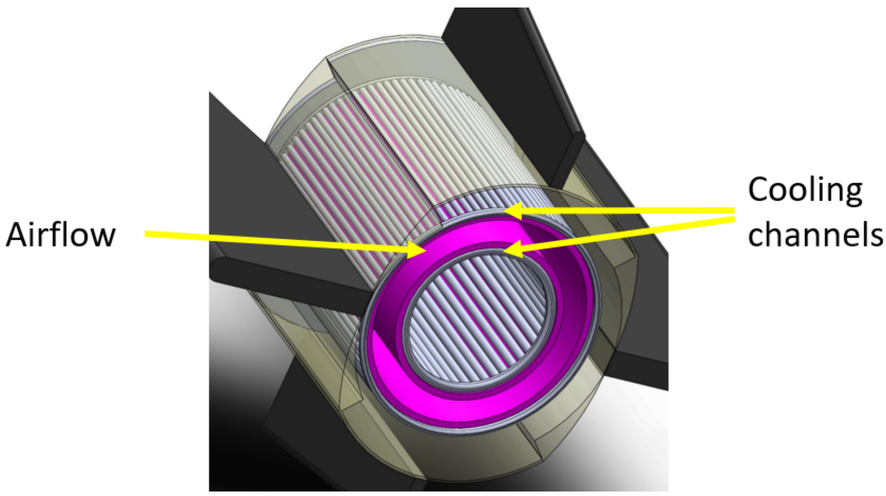

Figure 6: Combustor Geometry

Using the Stechmann model, the RDE's performance was analyzed across the flight conditions the vehicle would experience. During acceleration, an equivalence ratio of 1 was chosen to capitalize on performance while avoiding extreme temperatures. During cruise, the equivalence ratio was reduced to 0.58 in order to produce enough thrust for steady level flight. The performance characteristics of the RDE is shown in table EQ. Detailed plots of the predicted flow parameters between detonation fronts can be found in the appendix.

	Acceleration	Cruise
Isp(s)	2131-2219	2080
Thrust (N)	3076-1963	1007.19
Air Mass Flog (kg/s)	3.868-3.346	3.346
Fuel Mass Flow (kg/s)	0.262 - 0.227	0.131
Cf	1.61 - 1.67	1.664
C* (m/s)	1444	1326
Eq. Ratio	1	0.58
CJ Pressure Ratio	5.327 - 5.11	4.25
CJ Temperature Ratio	2.93 - 2.84	2.54
Combustor Mach	1.5 - 2.14	2.14
Entrance Pressure (kPa)	250 - 195	195

A major assumption made in this model is the ability for an RDE to be able to deep throttle from an equivalence ratio of 1 down to 0.58. Such a shift will affect the cell size and impose transients during throttling, of which neither effect has been studied in detail and remains an important question for the true capability of an RDE.

3.6 Nozzle [Gabriel Diez]

An aerospike nozzle design was chosen to expand the gases exiting the combustor and add additional thrust. Imbaratto [6] specifies a method to design the contour of an ideally expanded aerospike nozzle utilizing the Prandtl-Meyer function. The method starts by calculating the nozzle pressure ratio. Normally nozzles are designed for a combustor with a constant chamber pressure, however, in an RDE engine the pressure varies with time and location as a result of the travelling detonation wave. Therefore, the average pressure over the whole nozzle entrance area was calculated to be 365.8 kPa. Based on this pressure and the combustor exit Mach number and temperature of 2.14 and 2417 K, respectively, the Prandtl-Meyer function was solved to find the maximum turning angle of the flow at several points. A MATLAB program was then made to plot these points, developing the nozzle contour along the axial length from the combustor.

The result of this is shown in Figure 7 and it is apparent that the ideal contour leads to a long and sharp tip. While this thin tip does lead to perfect expansion to ambient pressure, it is impractical for several reasons. Manufacturing a shrinking spike with a precise geometry such as this would be difficult and the pointed end could be easily damaged. The main problem with the purely ideal aerospike nozzle, however, is heat transfer. Developing a system to effectively remove the heat being deposited in a 2 mm diameter pointed spike by supersonic gas at the high temperatures exhibited by a scramjet would be far too strenuous to justify the negligible improvement in expansion it would provide. The static pressure as a function of distance long the nozzle was then calculated and plotted in Figure 8. A point 127 mm in length and 25 mm in radius was chosen to truncate the nozzle as it would only leave the exiting flow with a static pressure of about 3 KPa above ambient which was deemed acceptable. The final nozzle design is displayed in Figure 9.

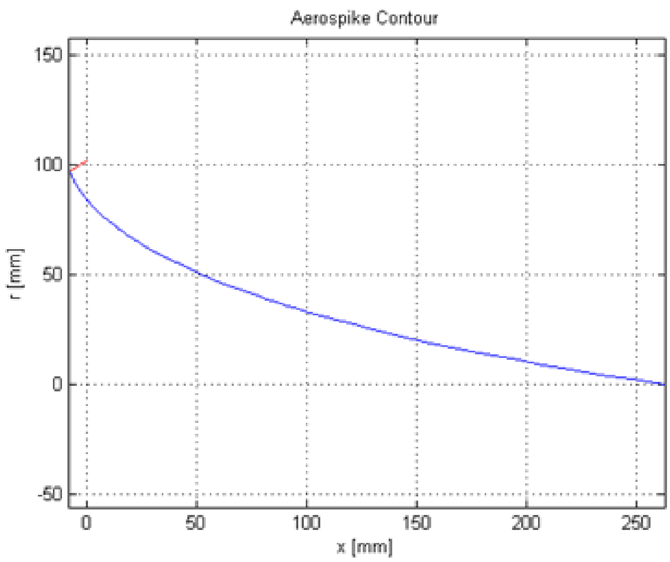

Figure 7: Aerospike Contour

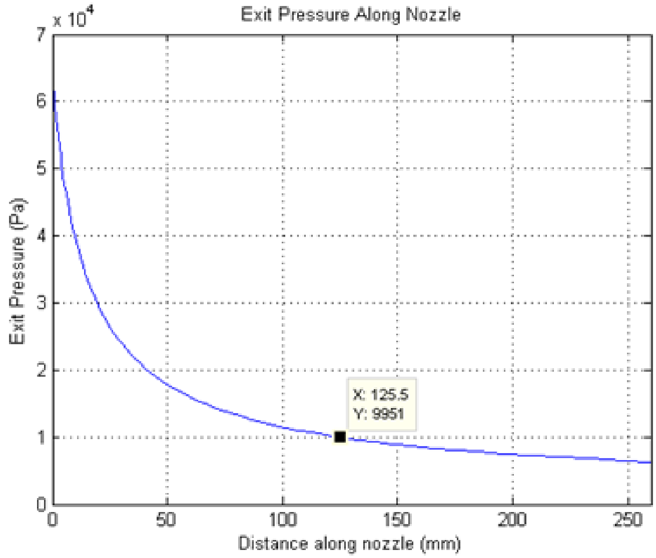

Figure 8: Pressure Along the Aerospike

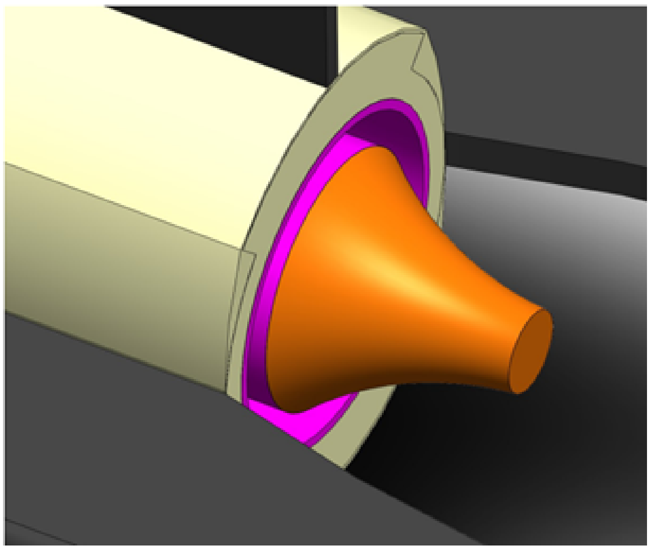

Figure 9: Final Nozzle Design

3.7 Heat Transfer

3.7.1 Combustor [Cameron Ellis]

The combustor consisted of a rotating detonation engine surrounded by an inner and outer wall that were each coated in TBC and regeneratively cooled. Heat transfer through the walls was calculated using a modified form of Bartz equation in order to calculate the heat transfer coefficient hg inside the combustor. Equation 10 shows the standard form of Bartz equation for a rocket nozzle.

$$h_g = \left[\frac{0.026}{D_t^{0.2}}\left(\frac{\mu^{0.2}C_p}{Pr^{0.6}}\right)_{ns}\left(\frac{(p_c)_{ns}g}{c^*}\right)^{0.8}\left(\frac{D_t}{R}\right)^{0.1}\right]\left(\frac{A_t}{A}\right)^{0.9}\sigma \tag{10}$$

Where the ns subscript denotes values of the gas inside of the combustor, and where sigma is the correction factor denoted by Equation 11.

$$\sigma = \frac{1}{\left[\frac{1}{2}\frac{T_{wg}}{(T_c)_{ns}}\left(1+\frac{\gamma-1}{2}M^2\right)+\frac{1}{2}\right]^{0.68}\left[1+\frac{\gamma-1}{2}M^2\right]^{0.12}} \tag{11}$$

For this combustor, there is no nozzle radius of curvature, denoted by R in the Bartz equation, so the term $\left(\frac{D_t}{R}\right)^{0.1}$ becomes 1. Furthermore, the area of the throat and the area of the combustor are equal since they have the same radius, so the area ratio term $\left(\frac{A_t}{A}\right)^{0.9}$ also becomes 1. Once an hg value was obtained, a guess at the hot side wall temperature, T_{wg} was taken and used to calculate heat flux from the combustor to the surface of the wall. This heat flux was then compared to the heat flux from the liquid coolant to the cold side of the wall, and compared together. The hot side wall temperature then changed iteratively until the two heat flux values matched. This was done across the entire length of the combustor, and was used to find the temperatures of the TBC inside the combustor, the temperature of the metal inside combustor wall, and the temperature of the ethylene in order to make sure boiling would not occur.

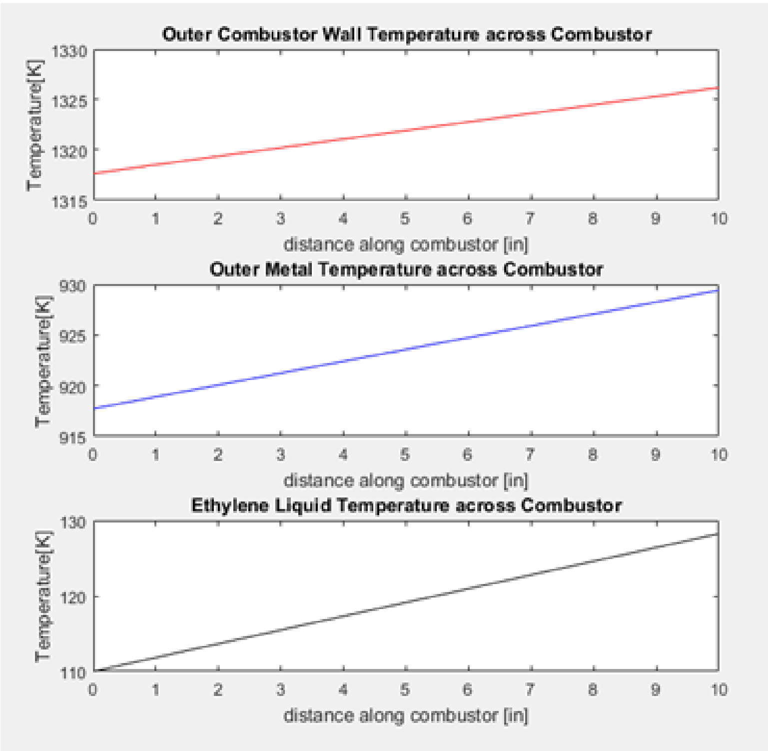

Figure 10: Temperature Range Across Combustor Structure

Figure 10 shows the temperature of the TBC, inside metal wall, and the ethylene across the length of the combustor. The TBC experiences temperatures of upwards of 1327 K at the hottest points after regenerative cooling is applied. The metal wall experiences up to 930 K, and therefore a material that could withstand those temperatures without going past its deformation temperature had to be selected. Incoloy 800 HT was chosen due to its high heat resistance. At the calculated temperatures, the alloy would be able to work at about 60% of its intended strength. The TBC coating selected was NAS3-23944, a super TBC created by NASA.

Figure 11 displays the elongation, tensile strength, and yield strength for INCOLOY 800HT for various temperatures. Though at the temperatures the RDE combustor would be operating at would affect the strength of the INCOLOY, it is still within a reasonable operating range for the metal work as intended.

To regeneratively cool both sides of the combustor, the mass flow rate of the liquid ethylene had to be split up between the inner and outer walls. Since the inner wall has a lower surface area, it would need less cooling channels, while the larger outer wall would need more. The cooling channels were split into 100 channels on the inner wall and 120 channels on the outer wall. Each cooling channel has a dimension of 0.215"x0.125" The mass split of the fuel ended up being 48.5% of fuel going to the inner regenerative cooling, and 51.5% of fuel going towards the outer regenerative cooling. This allows the two walls to experience approximately the same heat transfer, so the same thickness of thermal barrier coating would be able to be used on both sides. This was done to ensure that one side would not need to thick a layer of thermal barrier coating and increase the chance of cracking and flaking to take place during combustion.

3.7.2 Nozzle [Gabriel Diez]

The data used to design the ablative cooling system on the nozzle was taken from Tick et al [11]. In the study N2O4 and hydrazine were burned at 830 kPa and exhausted out of a nozzle coated with a 12.5 mm thick layer of silica phenolic ablative. Several parameters were varied in the experiment but in each test the fluid temperature exiting the combustor was 3144 K which lead to surface temperatures on the nozzle of 2644 K. Under these conditions, the time to char through the ablative as well as the erosion rate were measured. The time to char through was above 200s and the erosion rate never exceeded 0.05 mm/s. Since the total burning time of the RDE scramjet is 120 s and the gas temperatures never exceed 2500 K, it can be estimated that no more than 6 mm of ablative will be burned off. Therefore a design with a 12.5 mm thick layer of silica phenolic ablative coating similar to the one used in the Tick et al (1965) study was chosen since it had been proven experimentally to function under harsher conditions for a longer period of time. The ablative coating covers a metal interior support made of titanium for even further protection against any conductive heat transfer. A cross section of the ablative layer is displayed in Figure ( ).

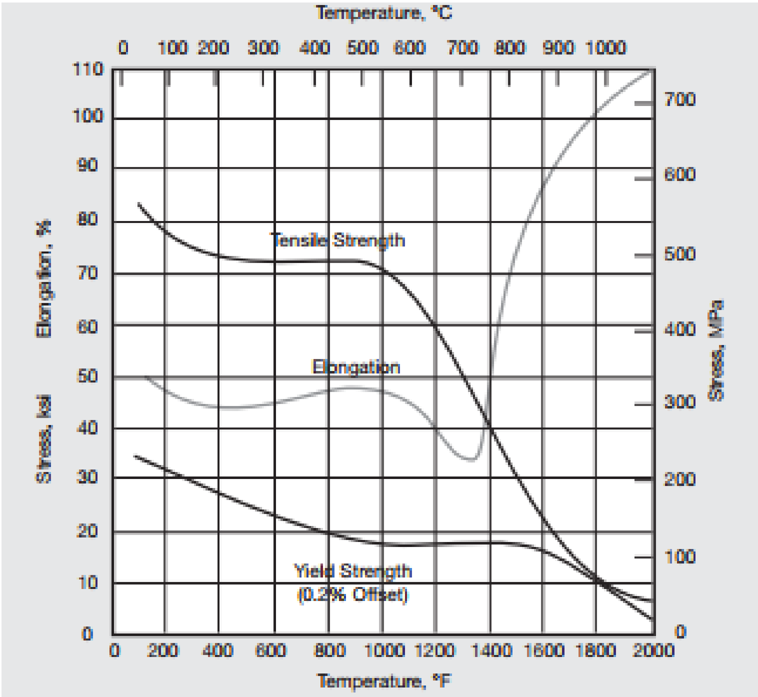

Figure 11: Temperature Range Across Combustor Structure [7]

3.7.3 Wings and Leading Edges [Alberto Marin Cebrian]

All the temperatures have been calculated for the steady state and for the most demanding operating conditions (cruise, Mach 6.5). The materials used in these exterior surfaces must tolerate high temperatures and a high emissivity is desirable. A higher emissivity will allow the material to reduce the maximum temperature it will have to withstand because it will be able to radiate more heat to the surroundings.

Inlet Cone Tip and Wing Leading Edges Infinitely thin surfaces and points are not possible to manufacture. Due to this fact a small normal shock will appear in front of these blunt bodies. This detached normal shock will create a huge deceleration of the flow and the properties of the flow will change significantly, it has been assumed that the air properties (γ in particular) will also change as the flow crosses the shock.

Properties after the shock allow us to calculate the Prandtl number at that location

$$Pr = \frac{(\mu_e Cp_e)}{K_e} = 0.4574 \tag{12}$$

Assuming that the boundary layer remains laminar, a similarity solution exists.

$$\frac{du_e}{dx} = \frac{1}{r_n}\sqrt{\frac{2(p_e - p_0)}{\rho_e}} \tag{13}$$

The recovery temperature depends on the Prandtl number. For laminar flows the recovery factor is r=sqrt(Pr)

$$T_r = T_e(1 + (\gamma_e - 1)/2\sqrt{Pr}M_e^2) = 2082K \tag{14}$$

Convective heat flux on the inlet cone tip The shape of the blunt cone is approximated to a semi-sphere. The heat flux is given by:

$$\dot{q} = 0.763Pr^{0.6}(\rho_e\mu_e)^{1/2}\sqrt{\frac{du_e}{dx}}Cp_e(T_r - T_w) \tag{15}$$

Convective heat flux on the wing leading edge The leading edge of the wing has a cylindrical shape with a nose radius equal to half of the thickness of the wing. The heat flux is also given by given by Equation 15.

Radiation heat flux The radiation heat flux has been calculated with the Stefan-Boltzman equation.

$$\dot{q}_{rad} = \sigma_s(\eta_w T_w^4 - T_0^4) \tag{16}$$

The steady state solution is reached when $\dot{q} = \dot{q}_{rad}$.

	Inlet Cone Tip	Wing Leading Edge
Nose Radius (m)	$1 * 10^{-3}$	$1.27 * 10^{-2}$
Temperature (K)	1962	1435
Material	Tantalum	Nichrome
Maximum Operating Temperature	3023	1573
Emissivity	0.225	0.89

The cone tip radius value has been estimated and based on the manufacturing tolerance it may change significantly. On the one hand, a bigger nose radius will decrease the temperature of the cone tip but it will decrease the performance of the inlet adding more drag. On the other hand, a smaller nose radius will be beneficial for the inlet performance but it will increase the temperature of the inlet cone. This value must be small enough not to affect significantly the inlet performance but big enough to be manufactured and get a temperature that lies inside the operating range of the material.

Wing Surface Temperature In order to obtain the temperature field over the wing of the aircraft the following assumptions have been made. The angle of attack of the vehicle is very small during the flight. This fact allows us to simplify the physics of the problem assuming that the angle of attack (α) is zero. In reality the angle will be different from zero and a compression oblique shock wave will appear for the lower part of the wing and an expansion wave will be developed in the upper surface. These waves will be very weak and will not change significantly the results of this analysis as soon as the angle of attack keeps being small enough. The wings are long and slender. Flat plate approximation has been used to calculate the heat fluxes at different sections of the wing. 1-D flow. The velocity of the flow can be simplified to $\overrightarrow{v} = (u, 0, 0)$.

Some important non-dimensional parameters that control the physics of this problem are the Reynolds number, the Prandtl number and the Nusselt number. The Reynolds number relates the inertial and viscous effects. It determines the change from laminar to turbulent flow in the boundary layer. For a flat plate, the transition Reynolds number from laminar to turbulent is 500,000.

$$\begin{aligned} Re_x = \frac{\rho u x}{\mu} & If Re_x < 500,000, \text{ Laminar boundary layer} \\ & If Re_x > 500,000, \text{ Turbulent boundary layer} \end{aligned} \tag{17}$$

The Prandtl is a dimensionless parameter representing the ratio of diffusion of momentum to diffusion of heat in a fluid.

$$Pr = \frac{\mu Cp}{K} \tag{18}$$

The recovery factor (r) depends on both, Prandtl number and Reynolds number.

$$\begin{aligned} r &= \sqrt{Pr} \text{ For laminar B.L.} \\ r &= Pr^{1/3} \text{ For turbulent B.L.} \end{aligned} \tag{19}$$

The Nusselt number is the ratio of convective hat transfer with respect to conduction. The Nusselt number depends on the other two dimensionless parameters (Prandtl number and Reynolds number).

$$Nu_x = \frac{h_g x}{K} \tag{20}$$

$$\begin{aligned} Nu_x &= 0.332\sqrt{Re_x} Pr^{1/3} \text{ For laminar flows} \\ Nu_x &= 0.0296 Re_x^{0.8} Pr^{1/3} \text{ For turbulent flows} \end{aligned} \tag{21}$$

With the Nusselt number and the axial position it is possible to obtain the convective heat transfer coefficient h_g.

$$h_g = \frac{K Nu_x}{x} \tag{22}$$

Note that this analysis is not valid for x=0 where the leading edge is located (h_g is infinite there). The convective heat flux is

$$\dot{q} = h_g(T_r - T_w) \tag{23}$$

Steady state is reached when the heat dissipated by radiation equals the heat inflow due to convection $\dot{q} = \dot{q}_{rad}$ In order to get the temperature contour of the wing, the wall temperature of the wing has been calculated in numerous locations along the wing.

3.8 Turbopump and Tank Sizing [Drew Sherman]

With cooling a serious issue in hypersonic aircraft, significant attention must be paid to the coolant used and its conditions. For the regenerative cooling system required by the aircraft's extreme thermal conditions, it becomes important to understand how the fuel, ethylene, behaves as it cools. One tactic used to ensure predictable and safe cooling is keeping the fuel above its critical point. Ethylene's critical point is about 5 MPa. Keeping coolant above its critical point theoretically eliminates boiling/two-phase flow concerns as the fuel is pumped over hot material, absorbing heat. The extreme pressure ensures that the liquid will not boil, even in extremely hot environments, which may or may not be seen. Unfortunately, keeping ethylene at this high of a pressure requires a significant initial pressurization and heavy tanks or an active pressurization system on the craft, operating during flight. A simple trade study was used to determine which method should be used to minimize overall system mass.

It is popular to load the fuel into craft at high pressure, which may be feasible depending on the margin allowed for tank weight. Tank weight is dependent upon the mass and density of the fuel stored and the pressure desired for the fuel in the tank. Standards from ASME [10] indicate a burst pressure of approximately three times storage pressure, which must be reflected in the weight. According to given conditions, the fuel tanks can achieve a ratio of $PV/W = 1e6in$. See the table below for specific sizing specifications:

	Value (SI)	Value (Imperial)
Ethylene Mass	21 (kg)	46.3 (lbm)
Tank Burst Pressure	21 (MPa)	3045 (psi)
Ethylene Storage Pressure	7 (MPa)	1015 (psi)
Ethylene Density	567.7 (kg/m^3	0.02051 (lbm/in^3
Tank Mass	3.2 (kg)	6.9 (lbm)

Initial aircraft sizing and design was based on a small turbopump system that was designed based on parameters from a paper developed by Blank et. all at Purdue University [2]. Figure 12 illustrates the major componenets of the turbopump system.

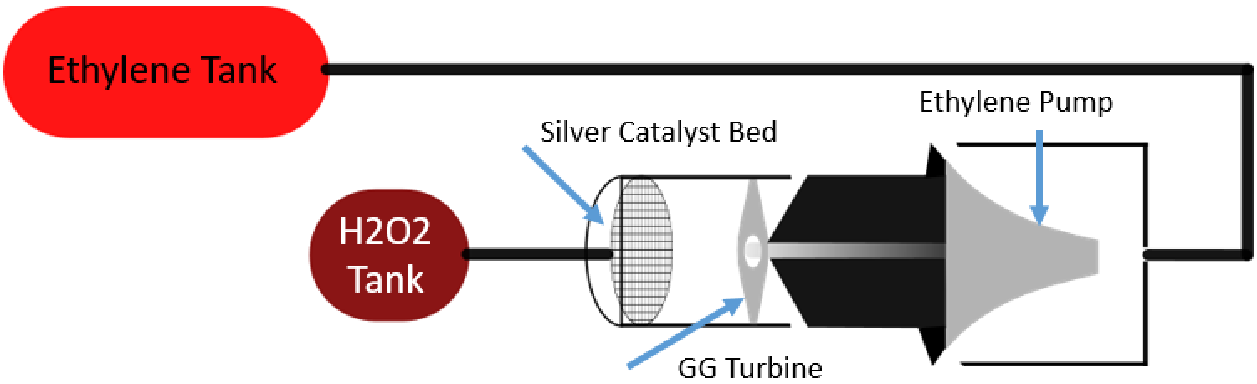

Figure 12: Turbopump System Illustration

The turbopump is driven by liquid rocket-grade (90%) hydrogen peroxide (lH2O2) . Sending the peroxide through a silver catalyst bed allows for decomposition and combustion. The products are sent through a small turbine used to drive a pump, raising ethylene pressure. The model is based off catalyst bed loading values and pressure drop values from Blank's paper [2]. The model uses NASA Chemical Equilibrium Analysis (CEA) to calculate the performance of the silver gas generator at various operating pressures. The rest of the system assumes certain pressure drops, including piping, cooling, and injection pressure losses. Using known and desired conditions for the ethylene, the model solves for the required peroxide massflow to run the pump at various operating pressures by balancing power requirements. Figure 13 the relationship between gas generator operating pressure and required massflow.

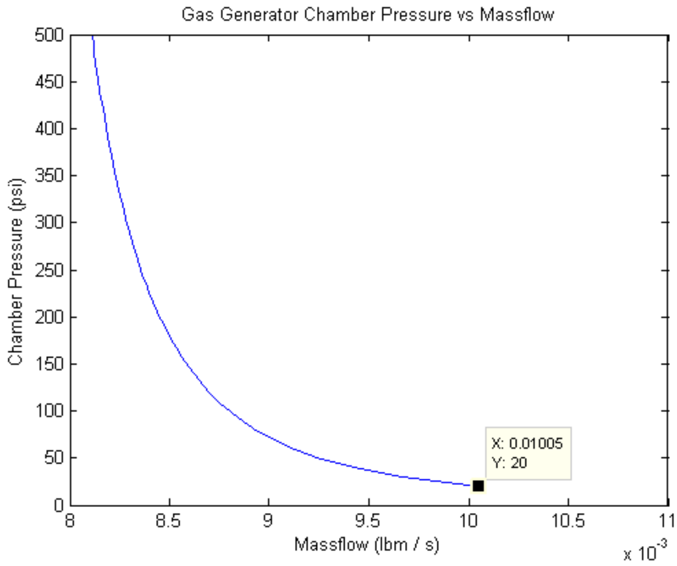

Figure 13: Turbopump Pressure v. Mass Flow Rate

As can be seen, gas generator chamber pressure affects the amount of peroxide required to drive the pump, but the peroxide massflow is still low. As such, its possible to run the gas generator at low chamber pressures to reduce chances of failure. In addition to solving for massflow, the model generates approximate sizing specifications required for the ethylene pump impeller given assumed performance requirements [5]. Given the relatively high performance of the pump, a strong material that can withstand low temperatures and high pressures is required. Research into rocket-grade turbopumps [8] shows that RENE 41 should be used for the walls and structure of the gas generator, turbine, and pump assembly due to its high-temperature capability and small thermal expansion[2]. The impeller. since it is estimated at spinning around 30,000 rpm, requires a strong material capable of handling low temperatures. Thus, a titanium alloy containing 5% aluminum and 2.5% tin is used, as it is capable of handling the temperature range and intermediate reactive products from the gas generator [5]. Sizing and performance characteristics of the gas-generator turbopump system are listed below:

Fuel Flowrate (kg/s)	0.13
H_2O_2 Flowrate (kg/s)	0.004
Total H_2O_2 Mass (kg)	0.75
Fuel dP (kPa)	7000
H_2O_2 Combustion Pressure (kPa)	345
Impeller Exit Radius (cm)	6
Impeller Inlet Radius (cm)	0.5
RPM	30,000
Wall Material	RENE 41
Iimpeller and Turbine Material	Titanium Alloy
Mass (kg)	5.3
Required Bed Area (cm^2)	0.15
Bed Loading ($lbm/s/in^2$)	0.4
Operating Power (HP)	3.2

The turbopump system is similarly sized to a typical turbocharger in a car, with higher performance.

With both pressurization methods analyzed, it becomes obvious that simply storing the ethylene at supercritical pressure results in less mass and less complexity. The turbopump assembly also takes up valuable volume in the center of the craft, which can be used for more fuel to extend range capability. If the required ethylene massflow were to approximately double, the turbopump system begins to show its strengths, especially since tank mass increases linearly with fuel mass.

4 Results

5 Conclusions

References

[1] MilStd 5007D.
General specification for engines, aircraft, turbojet, and turbofan, October 1973.

[2] R. A. Blank, T. L. Pourpoint, S. E. Meyer, S. D. Heister, and W. E. Anderson.
Experimental and Theoretical Performance of High-Pressure Hydrogen Peroxide Catalyst Beds, volume 28.
Journal of Propulsion and Power, 2012.

[3] D. C. Bull, J. E. Elsworth, P. J. Shuff, and E. Metcalfe.
Detonation Cell Structures in Fuel/Air Mixtures, volume 45.
Combustion and Flame, 1982.

[4] Fedor A. Bykovskii, Sergey A. Zhdan, and Evgenii F. Vedernikov.
Continous Spin Detonations, volume 22.
Journal of Propulsion and Power, November 2006.

[5] A. Csomor and R. Sutton.
Small, High-Pressure Liquid Hydrogen Turbopump.
Rockwell International, Canoga Park, CA, May 1977.

[6] David Michael Imbaratto.
The interaction between throttling and thrust vectoring of an annular aerospike nozzle.
mathesis, California Polytechnic State University, September 2009.

[7] Special Metals.
Incoloy alloy 800h & 800ht.
http://www.specialmetals.com/assets/smc/documents/alloys/incoloy/incoloy-alloys-800h-800ht.pdf.
Accessed: 2017-12-15.

[8] NASA, editor.
Liquid Rocket Engine Centrifugal Flow Turbopumps.
NASA SP-8109, December 1973.

[9] Brent Ruttle, Jacob Stork, and Glenn Liston.
Generic Hypersonic Vehicle for Conceptual Analyses.
Air Force Research Lab, 2012.

[10] Walter J. Sperko.
Reduction of design margin ("safety factor") in the asme boiler and pressure vessel code in the 1999 addenda.
Sperko Engineering, June 2000.

[11] S. J. Tick, G. R. Huson, and R. Griese.
Design of Ablative Thrust Chambers and Their Materials, volume 2.
AIAA Journal, May 1965.

[12] P. J. Waltrup and F. S. Billig.
Structure of Shock Waves in Cylindrical Ducts, volume 11.
AIAA Journal, 1973.

6 Appendix